Controlling the intensity statistics of speckle patterns: From normal to subthermal or superthermal distributions

Samuel B. Alves,[1] Hugo L. D. de S. Cavalcante,[2] Gilson F. de Oliveira Jr.,[3] Thierry Passerat de Silans,[4] Itamar Vidal,[5] Martine Chevrollier,[6,*] and Marcos Oriá[6]

[1]*Coordenação de Física, Instituto Federal do Sertão Pernambucano, Campus Salgueiro, BR232-Km504, 56000-000 Salgueiro, Pernambuco, Brazil*

[2]*Departamento de Informática, Universidade Federal da Paraíba, Avenida dos Escoteiros s/n, Mangabeira VII, 58055-000 João Pessoa, Paraiba, Brazil*

[3]*Instituto de Formação de Educadores, UFCA, 63260-000 Brejo Santo, Ceará, Brazil*

[4]*Departamento de Física/CCEN, Universidade Federal da Paraíba, Caixa Postal 5008, 58051-900 João Pessoa, Paraiba, Brazil*

[5]*LOQEF, 57039-739 Maceió Alagoas, Brazil*

[6]*UACSA, Universidade Federal Rural de Pernambuco, Cabo de Santo Agostinho, 54518-430 Pernambuco, Brazil*

(Received 19 October 2018; published 19 March 2019)

We study the propagation of speckle patterns in a tunable nonlinear medium. Starting from a spatial pattern of photons with a normal distribution (speckle field), we characterize the evolution of the radiation to either subthermal or superthermal distributions and demonstrate the control of this evolution through a single parameter. Our experimental control of the local degree of coherence of the output photons is well described by numerical simulations that consider both dispersive and absorptive nonlinear effects. Particularly, we analyze the role of the nonlinear absorption that either enhances or competes with the dispersive effects in the evolution of speckle fields. In some realizations, an asymptotic power law is observed in the photon spatial distribution.

DOI: 10.1103/PhysRevA.99.033838

I. INTRODUCTION

Many natural and artificial systems exhibit deviations from normal (Gaussian) statistics. Non-normal statistics have been observed, for instance, in biological [1,2], ecological [3], geological [4], behavioral [5,6], and economic [7] systems. Therefore, an increasing effort has been made to explain and eventually forecast such non-normal behaviors. Electronic [8] and optical [9] setups have been used as proxies for studying anomalous system properties. A large variety of issues in basic and applied sciences may be addressed by analyzing light propagation in different media. For example, rogue waves, an extreme phenomenon in sea waters, have been studied in optical systems [9–12]; Anderson localization has been associated with statistical properties of radiation, signaling conditions in which to observe wave localization in disordered media [13,14]; the statistical regime in random lasers is related to the inherent disorder of their gain medium [15–17]. More generally, photon propagation appears to be a well-adapted framework for studies of non-normal statistical behavior, a major signature of complex systems [5,8,18]. Moreover, there is an intrinsic interest in the description of the propagation of radiation in inhomogeneous media with implications in biology [19], medicine [20], and communications [21].

Propagation of light in inhomogeneous media exhibits a diversity of statistical behaviors because of particular spatial geometry [22] or spectral response of the medium [23]. In the latter case, studies have been performed by observing the anomalous spatial statistics [23,24] or the spectral evolution [25] of resonant photons scattered in an atomic vapor. In these works, the medium response was linear with the light intensity. Here, we report on the propagation of speckle fields in nonlinear (NL) media where propagating photons are described as interacting particles. The nature of the interaction, whether attractive or repulsive, as well as its strength, can be adjusted through a single control parameter, the radiation frequency, for instance. Changes in the spatial correlation of the interacting photons modify the spatial distribution of the light and, therefore, the statistics of spatial photon density.

A two-dimensional (2D) + 1 configuration is considered where the field $E(\vec{r}, \omega)$ propagates along one dimension (1D) (Oz) and is scattered on the plane perpendicular to (Oz), following the paraxial equation:

$$2ik\frac{\partial \mathbf{E}}{\partial z} = -\nabla_{\perp}^2\mathbf{E} - k^2\chi\mathbf{E}, \tag{1}$$

where $k = \omega/c$ is the vacuum wave number, $\nabla_{\perp}^2\mathbf{E}$ represents the transverse diffraction of the field in the medium, and $\chi = [\mathrm{Re}(\chi) + i\,\mathrm{Im}(\chi)]$ is the complex electric susceptibility of the medium, governing its interaction with the electromagnetic field.

The spatially random incident field is characterized through its intensity distribution $P(I_0)$ and propagates through the NL medium whose response depends on the (local) intensity of the field, thus creating a spatial pattern of index of refraction that determines the direction of scattering of the field itself. These dispersive effects are produced by the real

*Corresponding author: martine.chevrollier@ufrpe.br

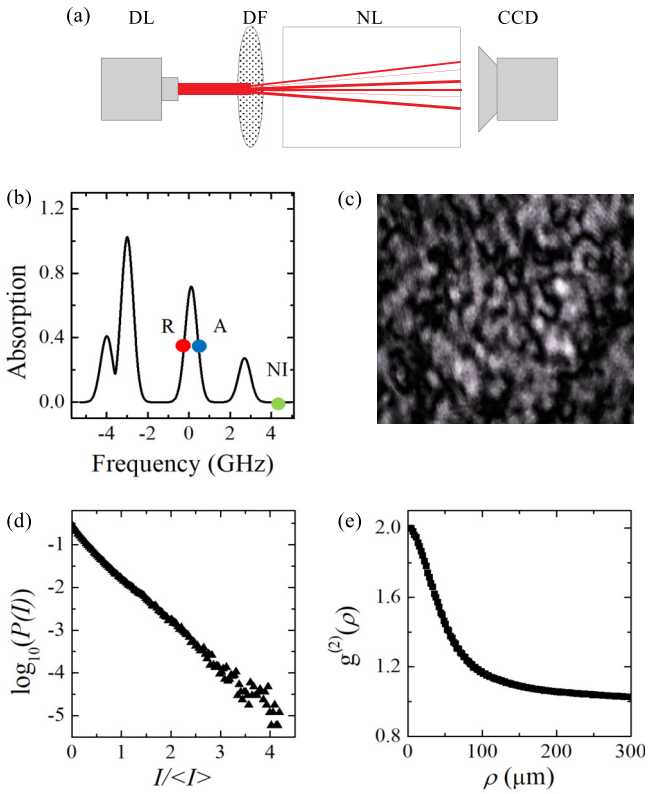

FIG. 1. (a) A pattern of speckles is created through scattering of a laser beam by a diffuser (DF) and is sent through a tunable NL medium. The outgoing pattern is recorded by a CCD camera. (b) Doppler spectrum of the Rb D_2 lines. The marked frequencies are those mostly used in this paper, exploring different regimes of photons interaction: R repulsive, A attractive, and noninteracting (NI). (c)–(e) The pattern is prepared with a normal distribution: (c) image, (d) intensity probability density function (PDF), and (e) intensity correlation function of the incident pattern.

part of the susceptibility, but an additional spatial modulation of the field amplitude (and thus of the self-lensing effect) is produced by the imaginary part of the susceptibility (nonlinear absorption). The statistical properties of the spatial pattern are analyzed at the output of the nonlinear medium, particularly through the building of its intensity distribution $P(I)$ and of the 2D intensity correlation,

$$g^{(2)}(\boldsymbol{\rho}) = \frac{\langle \int d^2\mathbf{r}\, I(\mathbf{r}) I(\mathbf{r}+\boldsymbol{\rho})\rangle}{\int d^2\mathbf{r} \langle I(\mathbf{r})\rangle \langle I(\mathbf{r}+\boldsymbol{\rho})\rangle}, \tag{2}$$

which gives information about the photons coherence [26,27] on the plane of the output pattern. In Eq. (2), the angular brackets $\langle\,\rangle$ denote averaging over many realizations.

II. EXPERIMENTAL SETUP

Experimentally, a speckle field is generated by a transparent diffuser that scatters a collimated laser beam [Fig. 1(a)]. The diffuser is designed in such a way as to yield a normal distribution of the field components, leading to an intensity PDF of the form [27]

$$P(I_0) = \frac{1}{\langle I_0\rangle} \exp\left(-\frac{I_0}{\langle I_0\rangle}\right), \tag{3}$$

where $\langle I_0\rangle$ is the average value of the input intensity distribution $I_0(\vec{r})$. Images of the pattern [Fig. 1(c)] are recorded by a CCD camera and analyzed (see Appendix B). The input light is normally distributed [Fig. 1(d)], and its intensity correlation function exhibits the shape expected for a normal distribution of field, varying from $g^{(2)}(\rho = 0) = 2$ to $g^{(2)}(\infty) = 1$ [Fig. 1(e)]. Here, $g^{(2)}(\rho)$ is the azimuthal average of $g^{(2)}(\boldsymbol{\rho})$ on a ring of radius $\rho = |\boldsymbol{\rho}|$. The width of $g^{(2)}(\rho)$ gives the mean size w of the speckles. This pattern characterization allows clear identification of subsequent modifications as due to the interaction with the NL medium.

The NL medium is a hot vapor of rubidium atoms of electric susceptibility $\chi(\Delta, I)$, where $\Delta = \omega - \omega_0$ is the detuning of the light field from the center of a Rb transition and $I(\vec{r}) = |E|^2$ is the intensity of the light at position $\vec{r}$ in the vapor. The frequency of the light field can be tuned around the D_2 resonant lines of Rb ($\lambda = 780$ nm, more experimental details in Appendix A). We show in Fig. 1(b) a typical absorption spectrum of a low-intensity light through a cell filled with a natural mixture of ^{85}Rb and ^{87}Rb atoms, exhibiting the four Doppler-broadened transitions available in our experiment. Both the real and the imaginary parts of χ have a strong spectral and intensity dependence around the central frequency of atomic transitions [28,29].

At frequencies below line center [red spot R in Fig. 1(b)], the dependence of the real part of the susceptibility with intensity results in a repulsive interaction between photons as inferred from the fact that self-defocusing spreads the light away from the regions where the photon density is larger. Conversely, at frequencies above line center, high-intensity light is focused, equivalent to an attractive interaction between photons [blue mark A in Fig. 1(b)]. Far from resonance [green mark NI in Fig. 1(b)], the refractive index does not depend on the intensity and the photons do not "interact."

III. PROPAGATION SIMULATIONS

Numerical simulations of the propagation of the speckles field allow us to follow the evolution of the intensity statistics all along the nonlinear medium, whereas experiments are conducted in fixed-length samples. Simulations also allow us to gain insight into the effects of the NL absorption as these can be artificially suppressed or enhanced on demand.

The initial field $E_0(x, y, 0)$ follows a normal probability distribution [Eq. (3)] and propagates [Eq. (1)] through the medium, assumed to be composed of two-level atoms with the NL susceptibility:

$$\chi(\Delta, I) = \frac{1}{u\sqrt{\pi}} \int_{-\infty}^{+\infty} \chi(\Delta, I, v) e^{[-(v/u)]^2} dv, \tag{4}$$

with

$$\chi(\Delta, I, v) = -\frac{2N|\mu^2|}{\epsilon_0 \hbar \Gamma^2} \frac{2(\Delta - kv) - i\,\Gamma}{1 + 4\frac{(\Delta - kv)^2}{\Gamma^2} + I/I_{\text{sat}}}. \tag{5}$$

In Eqs. (4) and (5), v is the velocity in the direction of propagation z, u is the most probable velocity, N is the atomic

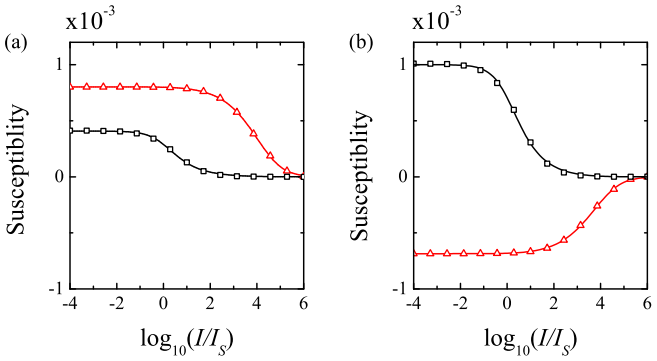

FIG. 2. Real (red-solid line) and imaginary (black-solid line) parts of the Doppler-integrated susceptibility of the Rb vapor, calculated from Eq. (4) as a function of the intensity. The diamonds (squares) are the best fit of the real (imaginary) curve by the function F in Eq. (6). (a) $\Delta = -400$ MHz and (b) $\Delta = +200$ MHz.

number density, μ is the atomic dipole moment, ϵ_0 is the vacuum permittivity, $h = 2\pi\hbar$ is Planck's constant, Γ is the homogeneous linewidth, λ is the wavelength of the atomic transition, and $I_{\rm sat}$ is its saturation intensity.

The susceptibility strongly varies with the local intensity $I(\vec{r})$ and *explicit* determination of $\chi(I)$ is essential in the calculation of the propagation of the nonuniform field. In other words, one cannot use a mean value of intensity to propagate a speckle pattern through a NL medium. In order to simplify the resolution of Eq. (1), Eq. (4) is numerically integrated beforehand for a given detuning Δ, and the curves $\mathrm{Re}[\chi(\Delta, I)]$ and $\mathrm{Im}[\chi(\Delta, I)]$ are fitted by an analytical expression of the form

$$F(\mathcal{J}) = \frac{A_k}{B_k + C_k \mathcal{J}^{E_k}} e^{D_k \mathcal{J}}, \tag{6}$$

where $\mathcal{J} = I/I_S$, $\{A_k, B_k, C_k, D_k, E_k\}$ is a set of constants for a given detuning Δ, and the index $k = r, i$ stands for the real and the imaginary parts of χ, respectively. The dependence of χ with the intensity, for detunings $\Delta = -400$ MHz [$\mathrm{Re}(\chi) > 0$, repulsive photon interaction] and $+200$ MHz [$\mathrm{Re}(\chi) < 0$, attractive interaction], is shown in Fig. 2 with its corresponding fit by Eq. (6).

We solve Eq. (1) by using for χ the value given by the function $F(\mathcal{J})$ of the local intensity and thus simulate the reciprocal induction between the light and the medium properties [$\chi(I) \rightleftharpoons I(\mathrm{Re}\,\chi, \mathrm{Im}\,\chi)$] along the whole length of the resonant vapor. Experimentally, we only have access to the distribution at the exit window of the cell.

The relatively short polarization lifetime of atoms under high intensities and densities allows us to neglect possible nonlocal effects, and we assume a local relationship between the nonlinear index of refraction of the medium and the intensity of the light.

IV. RESULTS

A. From normal to sub- or super-thermal

Figure 3 shows the experimentally measured and the numerically calculated histogram and correlation function of the speckles intensity in three regimes of interaction. The

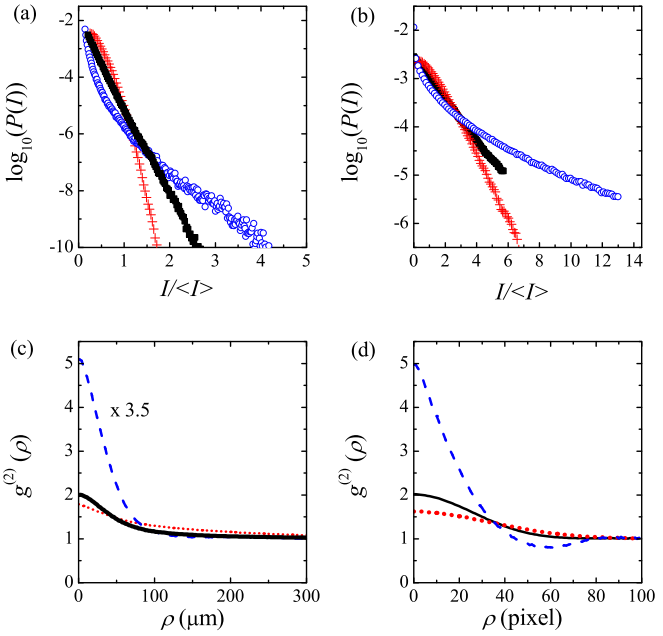

FIG. 3. (a) Experimentally measured and (b) calculated PDF of the intensity of the speckle pattern after propagation through the NL medium. $\langle I \rangle$ is the mean intensity of the distribution. (c) Experimentally measured and (d) calculated correlation function of the intensity of the speckle pattern after propagation through the NL medium. The actual magnitude of the experimental $g^{(2)}$ in the attractive regime has been divided by 3.5. Noninteracting (off-resonance laser, black-thick curve), attractive (positive detuning, blue-empty circles/dashed curve), and repulsive (negative detuning, red crosses/dotted curve) regimes, see Fig. 1(b).

horizontal scale of the histograms is normalized to $\langle I \rangle$, the mean intensity of *each* distribution.

For noninteracting photons, the intensity PDF [thick black curves in Figs. 3(a) and 3(b)] decays exponentially with I as does the input field, i.e., there is no change in the intensity statistics. This is confirmed by the intensity correlation function [black-solid lines in Figs. 3(c) and 3(d)], which assumes the same shape as $g^{(2)}(\rho)$ of the input field.

Attractive photon interaction favors the formation of high-intensity speckles. This increase in the probability of high-value events is characteristic of a superthermal distribution [blue-circle curves in Figs. 3(a) and 3(b)]. The Gaussian-like shape of the correlation function of the incident field evolves to a sharper, narrower peak in the attractive regime with $g^{(2)}(0)$ becoming much larger than 2 [dashed-blue lines in Figs. 3(c) and 3(d)].

Tuning to repulsive interactions leads to subthermal distributions [red-cross curves in Fig. 3(a) and 3(b)] with an intensity cutoff reflecting the suppression of the highest intensities from the normal distribution. On the other hand, the probability of intermediary intensities exceeds that of the exponential decay, which turns the overall field distribution more uniform as can be verified by correlation measurements. The decrease (below 2) in $g^{(2)}(0)$ in this repulsive regime is accompanied by the increase in the mean speckle size w, measured by the width of $g^{(2)}(\rho)$ [dotted-red lines in Figs. 3(c)

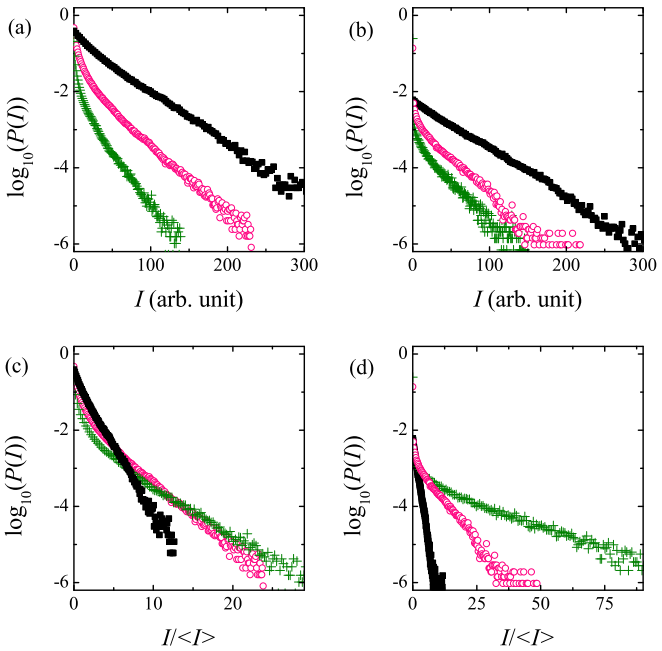

FIG. 4. Intensity histogram of the speckles pattern resulting from propagation in a purely absorbing NL medium for the laser tuned at the line center of two different Rb transitions. (a) and (c) Experimental and (b) and (d) calculated histograms. ^{85}Rb $F = 3 \rightarrow F'$, green crosses; ^{85}Rb $F = 2 \rightarrow F'$ magenta-empty circles; noninteracting, black-filled squares. (a) and (b) $P(I)$; (c) and (d) the horizontal scale is normalized to $\langle I \rangle$, the mean intensity of each distribution.

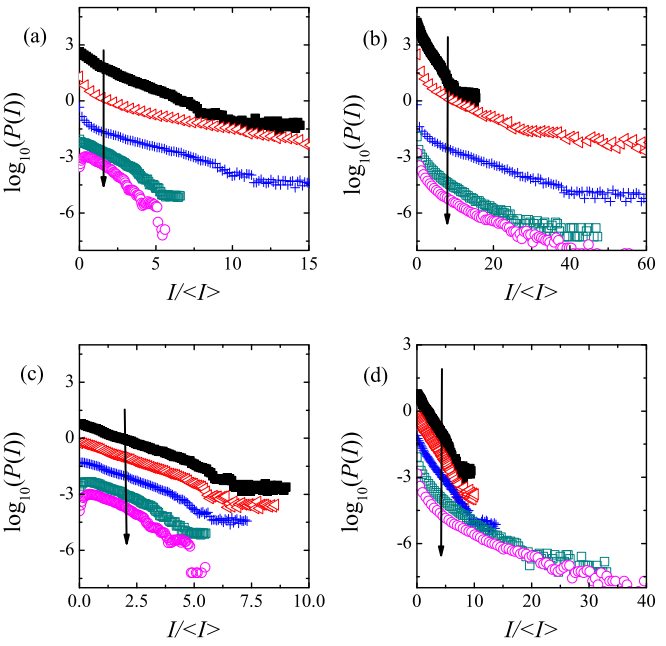

FIG. 5. (a) and (b) Calculated intensity PDF of an initially Gaussian speckles pattern after propagation in a NL medium exhibiting both real and imaginary indices of refraction for a few incident intensities (0.1; 1.0; 10.0; 100.0; 500.0 mW/cm^2). (a) Frequency on the red side and (b) frequency on the blue side of the ^{85}Rb $F = 2 \rightarrow F'$ transition. (c) Calculated PDF taking into account only dispersion for the same detuning and incident intensities as (a). (d) Calculated PDF taking into account only dispersion for the same detuning and incident intensities as (b). The arrows indicate increasing power.

and 3(d)] due to the larger spots as a result of a more uniform pattern of intensities.

This general behavior was also observed with other nonlinear materials [30] either in 1D + 1 or 2D + 1 configurations. Here, using sharp resonances we are able to sweep easily between subthermal and superthermal intensity distributions. This ability to finely control the output pattern statistics is the main result of this paper.

B. Role of the non-linear absorption

Studies of NL effects of propagating fields usually avoid describing absorption. The interpretation is then performed through the nonlinear Schrödinger equation where only dispersion, eventually competing with diffraction, yields NL behaviors, such as solitons [31]. Absorption, however, may play a non-negligible role in real systems and may, for example, contaminate the signature of Anderson localization of photons in three-dimensional disordered materials [13]. Our system naturally exhibits a large absorption. Effects of the NL absorption influence the propagation of the radiation in the medium, modifying the intensity statistics and degree of coherence and diverting them from normal behavior. Both absorptive and dispersive effects are therefore at work in the statistical behaviors exhibited in the experimental and numerical distributions discussed in the previous session. The NL absorption may be isolated by tuning the laser frequency to line center where dispersion vanishes. Intensity histograms for hyperfine transitions of Rb with different absorption coefficients are shown in Fig. 4 as well as the normal input histogram. At the line center, the probabilities of all intensities are reduced below their normal value by absorption. As nonlinear absorption does not equally reduce all the intensities, it enhances the contribution of the highest intensity values, resulting in a probability distribution for the transmitted field [Figs. 4(c) and 4(d)] that is qualitatively equivalent to the attractive regime [see blue-circle curves in Figs. 3(a) and 3(b)].

In general (for frequencies close to resonance), the effects of nonlinear absorption and dispersion combine to shape the evolution of the field and its statistics. Experimentally, we cannot extinguish NL absorption. Numerical simulations, however, allow us to cancel absorption and clearly evidence the dispersion-induced changing of the interaction regime, from repulsive to attractive, as the frequency is swept across the resonance center. Simulations show, as expected, that the competition between dispersive and absorptive effects is particularly observable in the red wing of the resonance where dispersion leads to repulsive effects. At low nonsaturating incident power, all intensities but the very highest ones are equally absorbed, and the output intensity PDF reproduces the normal input distribution with a far-range fat tail due to high intensities being less absorbed than the others [Fig. 5(a), black curve]. As power is increased, more intensities in the input distribution fall in the region where dispersion is still linear, whereas the absorption is already essentially nonlinear (see Fig. 2): Low-saturated absorption of low-to-medium intensities distorts the overall distribution by increasing the relative contribution of high intensities [Fig. 5(a), red-empty

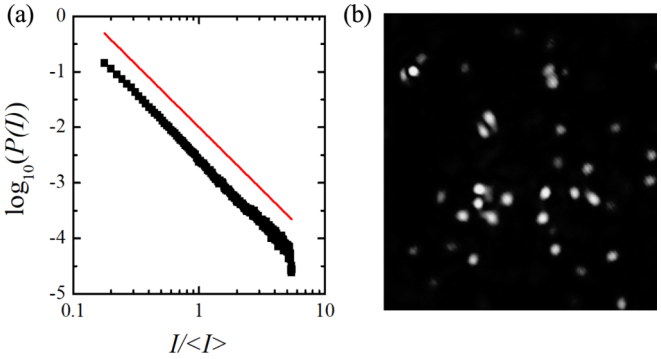

FIG. 6. (a) PDF of the intensity on a $\log_{10}$-$\log_{10}$ scale: power-law regime. In this strongly attractive regime $P(I)$ decays as $\alpha = -2.4$. See the parallel line to guide the eyes. (b) Speckle pattern output from the nonlinear medium in the very strong attractive regime. The symmetrical spots are the areas of collapse [33].

diamond and blue-cross curves]. NL absorption makes thus the repulsive case less subthermal than the sole dispersive effects as seen in Fig. 5(c). Finally, as power is further increased, the input intensity distribution shifts to the high-intensity region where dispersion overcomes absorption and the output intensity PDF exhibits the behavior described in the precedent sections where the subthermal regime was clearly evidenced [Fig. 5(a), green-empty-square and magenta-empty-circle curves]. In the blue wing of the resonance, on the contrary, absorptive effects enhance dispersive ones and make the repulsive case more superthermal than the sole dispersive effects, see Fig. 5(d).

C. Power-law intensity distribution

Nonlinearity associated with spatial symmetry breaking has been shown to lead to long-tail statistics [32]. Here, the spatial modulation of the nonlinearity is granted by the speckle structure of the incident field and, in the attractive regime, results in long-tail intensity PDFs (see Fig. 3 for the attractive case). In some of the realizations with the highest incident power ($\approx$100 mW and beam diameter $\approx$3 mm), and in the attractive regime, we have observed a PDF asymptotically following a power-law $P(I) \propto I^{-\alpha}$ as shown in Fig. 6 where the PDF graph is on a $\log_{10}$-$\log_{10}$ scale evidencing $\alpha < 3$.

Moreover, in this strongly attractive regime, we observe that the incident (normal) random pattern converges to a small number of spots, each one presenting a rather symmetric shape [see Fig. 6(b)], suggesting that they may be in or close to the condition of wave collapse [33].

Our numerical simulations yield power laws with exponent $\alpha \approx -1.5$, whereas the observed power is closer to -2.5. Further refinement of the model may improve quantitative agreement with the measurements. Indeed, complex processes occurring in dense atomic vapors irradiated by a resonant radiation field have not been taken into account and may play a non-negligible role in the redistribution of intensity. Particularly, the two-level atom used in our model has been proven [28] to yield underestimated values of the Kerr coefficient in relation to a model involving the hyperfine structure of the excited state. To a lesser extent, inelastic processes, frequency redistribution, and modulation of the saturation intensity through interatomic collisions, radiation trapping [25], and optical pumping, may also affect the statistics of intensity in the NL medium.

V. CONCLUSIONS

In conclusion, we studied the propagation of a spatially random field through a tunable nonlinear medium where the incident field is prepared as a speckle pattern with Gaussian distribution of intensity. The nonlinearity of the medium creates correlations between the propagating photons that can be turned attractive, repulsive, or neutral depending on the frequency of the radiation. As a result, the statistical properties of the outgoing field can be strongly modified in a controlled way, so as to result in superthermal or subthermal statistics or to maintain the original thermal statistics. Our findings eventually open the way to applications, such as controlling the degree of coherence of a field for imaging purpose [34,35] or controlling speckle fields for particle manipulation [36,37].

ACKNOWLEDGMENTS

The authors acknowledge financial support from Conselho Nacional de Desenvolvimento Científico e Tecnológico (CNPq), Coordenação de Aperfeiçoamento de Pessoal de Nível Superior (CAPES), Fundação Cearense de Apoio ao Desenvolvimento Científico e Tecnológico (FUNCAP) (Grant No. BP3-0139-00360.01.00/18), and Financiadora de Estudos e Projetos (FINEP).

APPENDIX A: EXPERIMENTAL DETAILS

The radiation source is a cw Fabry-Pérot-type diode laser, emitting at 780 nm in resonance with the D_2 transition of Rb. The laser operates with a stable injection current ($\sim$140 mA) and junction temperature around 22 °C, delivering a total optical power of about 100 mW in most of the experiments. The mean diameter of the beam is 2.7 mm. The available power is reduced by losses, mainly due to the use of an optical isolator at the laser output and to the diffuser reflections and absorptions. The available power after the diffuser is about 65 mW. The commercial diffuser, placed at a distance of 5 cm of the cell input window, breaks the spatial coherence of the laser beam, scattering radiation in different directions [Fig. 1(a)] within an angle of divergence of 1° for most of the experiments in this paper. An example of the speckles' pattern generated by the interference from the multiple fields scattered by the diffuser is shown in Fig. 1(c). It has a random Gaussian statistical distribution. The speckles' pattern passes through a cylindrical optical cell with 1-cm length and 1-cm radius. A drop of Rb is deposited in the cell reservoir, whose temperature determines the vapor pressure and the density of atoms in the cell body. The cell is placed in an oven with optical windows. The body and the reservoir of the cell are heated independently, allowing control of the vapor density and keeping a temperature gradient between the cell body and the reservoir (temperatures around 140 °C and 120 °C, respectively). The slight overheating of the cell body ensures

that there is no condensation of the alkali atoms on the cell windows. The reservoir temperature of 120 °C corresponds to a pressure of 8×10^{-4} Torr and an atomic density of 2×10^{19} atoms/m^3.

APPENDIX B: DETERMINATION OF THE INTENSITY DISTRIBUTION

The speckle pattern at the exit of the optical cell is imaged onto the CCD through a unitary-magnification configuration (5-cm-focal-length lens inserted between the cell exit window and the CCD detector). The CCD sensor is constituted of 1600×2560 pixels of 2.2-μm side length, smaller than the average size of the speckles, on the order of a few tens of micrometers. Neutral filters are used, along with control of exposure time, to ensure that the detection is performed in the linear regime of the CCD camera. For each image we build normalized histograms $N_k(\mathcal{I})$ of the number of pixels N_k receiving a given level $\mathcal{I}$ of intensity (between zero and 255). We also calculate the correlation function of intensity for the two-dimensional image. An azimuthal average yields the intensity correlation as a function of the distance between pixels. The PDF and the correlation function of the intensity in a given configuration (incident power and frequency of the input light) are calculated by averaging over 50 images. For each image, the laser beam incides on a different zone of the diffusor, which is rotated from one image to the next, i.e., the averaging is carried out over 50 different realizations of random phases of the field scattered by the diffuser.

[1] M. J. Saxton, Biophys. J. **81**, 2226 (2001).
[2] M. J. Saxton, Biophys. J. **92**, 1178 (2007).
[3] G. Ramos-Fernández, J. L. Mateos, O. Miramontes, G. Cocho, H. Larralde, and B. Ayala-Orozco, Behav. Ecol. Sociobiol. **55**, 223 (2004).
[4] S. M. Burroughs and S. F. Tebbens, Pure Appl. Geophys. **158**, 741 (2001).
[5] D. Brockmann, L. Hufnagel, and T. Geisel, Nature (London) **439**, 462 (2006).
[6] G. M. Viswanathan, M. G. Da Luz, E. P. Raposo, and H. E. Stanley, *The Physics of Foraging: An Introduction to Random Searches and Biological Encounters* (Cambridge University Press, Cambridge, U.K., 2011).
[7] R. N. Mantegna and H. E. Stanley, Nature (London) **376**, 46 (1995).
[8] H. L. D. S. Cavalcante, M. Oriá, D. Sornette, E. Ott, and D. J. Gauthier, Phys. Rev. Lett. **111**, 198701 (2013).
[9] S. Birkholz, C. Brée, A. Demircan, and G. Steinmeyer, Phys. Rev. Lett. **114**, 213901 (2015).
[10] D. Solli, C. Ropers, P. Koonath, and B. Jalali, Nature (London) **450**, 1054 (2007).
[11] C. Bonatto, M. Feyereisen, S. Barland, M. Giudici, C. Masoller, J. R. R. Leite, and J. R. Tredicce, Phys. Rev. Lett. **107**, 053901 (2011).
[12] N. Akhmediev, J. M. Dudley, D. Solli, and S. Turitsyn, J. Opt. **15**, 060201 (2013).
[13] A. Chabanov, M. Stoytchev, and A. Genack, Nature (London) **404**, 850 (2000).
[14] M. Segev, Y. Silberberg, and D. N. Christodoulides, Nat. Photonics **7**, 197 (2013).
[15] R. Uppu and S. Mujumdar, Phys. Rev. A **87**, 013822 (2013).
[16] S. Lepri, S. Cavalieri, G.-L. Oppo, and D. S. Wiersma, Phys. Rev. A **75**, 063820 (2007).
[17] A. S. L. Gomes, E. P. Raposo, A. L. Moura, S. I. Fewo, P. I. R. Pincheira, V. Jerez, L. J. Maia, and C. B. de Araújo, Sci. Rep. **6**, 27987 (2016).
[18] C. Song, Z. Qu, N. Blumm, and A.-L. Barabási, Science **327**, 1018 (2010).
[19] D. D. Nolte, *Optical Interferometry for Biology and Medicine* (Springer, New York, 2011), Vol. 1.
[20] S. S. Kazmi, L. M. Richards, C. J. Schrandt, M. A. Davis, and A. K. Dunn, J. Cereb. Blood Flow Metab. **35**, 1076 (2015).
[21] L. C. Andrews and R. L. Phillips, *Laser Beam Propagation Through Random Media* (SPIE, Bellingham, WA, 2005), Vol. 52.
[22] P. Barthelemy, J. Bertolotti, and D. S. Wiersma, Nature (London) **453**, 495 (2008).
[23] N. Mercadier, W. Guerin, M. Chevrollier, and R. Kaiser, Nat. Phys. **5**, 602 (2009).
[24] M. Chevrollier, Contemp. Phys. **53**, 227 (2012).
[25] J. C. de A. Carvalho, M. Oriá, M. Chevrollier, H. L. D. de Souza Cavalcante, and T. Passerat de Silans, Phys. Rev. A **91**, 053846 (2015).
[26] J. Ohtsubo, J. Opt. **12**, 129 (1981).
[27] J. Goodman, in *Laser Speckle and Related Phenomena* edited by J. C. Dainty (Springer, Berlin/Heidelberg, 2013), Chap. 2, pp. 9–75.
[28] M. O. Araújo, H. L. D. de S. Cavalcante, M. Oriá, M. Chevrollier, T. P. de Silans, R. Castro, and D. Moretti, Phys. Rev. A **88**, 063818 (2013).
[29] P. Siddons, C. S. Adams, C. Ge, and I. G. Hughes, J. Phys. B: At., Mol. Opt. Phys. **41**, 155004 (2008).
[30] Y. Bromberg, Y. Lahini, E. Small, and Y. Silberberg, Nat. Photonics **4**, 721 (2010).
[31] J. Aitchison, A. Weiner, Y. Silberberg, M. Oliver, J. Jackel, D. Leaird, E. Vogel, and P. Smith, Opt. Lett. **15**, 471 (1990).
[32] D. Pierangeli, F. Di Mei, C. Conti, A. J. Agranat, and E. DelRe, Phys. Rev. Lett. **115**, 093901 (2015).
[33] K. D. Moll, A. L. Gaeta, and G. Fibich, Phys. Rev. Lett. **90**, 203902 (2003).
[34] A. P. Mosk, A. Lagendijk, G. Lerosey, and M. Fink, Nat. Photonics **6**, 283 (2012).
[35] B. Redding, M. A. Choma, and H. Cao, Nat. Photonics **6**, 355 (2012).
[36] D. Boiron, C. Mennerat-Robilliard, J.-M. Fournier, L. Guidoni, C. Salomon, and G. Grynberg, Eur. Phys. J. D **7**, 373 (1999).
[37] G. Volpe, G. Volpe, and S. Gigan, Sci. Rep. **4**, 3936 (2014).